JGR Oceans

RESEARCH ARTICLE
10.1029/2018JC014614

Multidecadal Wind Variability Drives Temperature Shifts on the Agulhas Bank

Neil Malan[1,2,3,4], **Jonathan V. Durgadoo**[5], **Arne Biastoch**[5], **Chris Reason**[2], **and Juliet Hermes**[1,2,6]

[1]SAEON Egagasini Node, Cape Town, South Africa, [2]Department of Oceanography, University of Cape Town, Cape Town, South Africa, [3]Nansen-Tutu Centre for Marine Environmental Research, University of Cape Town, Cape Town, South Africa, [4]Now at Coastal and Regional Oceanography Laboratory, School of Mathematics and Statistics, University of New South Wales, Sydney, NSW, Australia, [5]GEOMAR Helmholtz Centre for Ocean Research Kiel, Kiel, Germany, [6]School of Environmental Science, Nelson Mandela University, Port Elizabeth, South Africa

Key Points:
- A regional ocean model is used to examine multidecadal shelf temperature changes on the Agulhas Bank
- There are distinct shelf temperature regime changes in 1966 and 1996
- These regime shifts are caused by changes in coastal upwelling linked to large-scale wind variability

Correspondence to:
N. Malan,
neilcmalan@gmail.com

Citation:
Malan, N. C., Durgadoo, J. V., Biastoch, A., Reason, C. J., & Hermes, J. C. (2019). Multidecadal wind variability drives temperature shifts on the Agulhas Bank. *Journal of Geophysical Research: Oceans*, *124*, 3021–3035. https://doi.org/10.1029/2018JC014614

Received 29 SEP 2018
Accepted 9 APR 2019
Accepted article online 15 APR 2019
Published online 8 MAY 2019

Abstract The Agulhas Bank is an important area for the spawning of small pelagic fish and other species. Here, within a NEMO ocean model, we investigate changes in temperature over the Bank on multidecadal time scales. In agreement with previous observational studies, a shift to colder temperatures is found in 1997. The model also simulates an earlier shift from colder to warmer temperatures in 1966. These shifts are coastally confined and shown, using a climatologically forced model run as a control, to be driven by a north-south migration in the large-scale wind belts, rather than by changes in downward heat fluxes or changes in the Agulhas Current itself. The zonal wind changes on the Agulhas Bank show a significant relationship with the Southern Annular Mode, showing some promise for future predictability of cold and warm regimes on the Agulhas Bank. Thus, while the Agulhas Current has been shown in previous work to have a large impact on intra-annual and interannual temperature variability, this work shows that multidecadal variability in temperature on the shelf is likely to be wind forced.

1. Introduction

The Agulhas Bank is a wide, triangular-shaped area of shallow shelf on the southern tip of Africa. The western Agulhas Bank forms the southern limit of the Benguela upwelling system (Blanke et al., 2009), while the eastern Agulhas Bank forms the largest shelf region inshore of the Agulhas Current. The Bank is approximately 800 km east to west (18–29°E) and 250 km wide at its widest north-south extent, covering some 116,000 km^2 (Figure 1). The Agulhas Bank is analogous to other east coast shelf systems inshore of western boundary currents, such as the north-east shelf of the United States or the shelf regions inshore of the Brazil Current (Hutchings, 1994). Early observational work (Chapman & Largier, 1989; Largier & Swart, 1987; Swart & Largier, 1987) shows a strong thermocline, deepening from east to west. The sloping of this thermocline is due to the change from an advectively controlled thermocline in the eastern Agulhas Bank, strongly influenced by the Agulhas Current (Jackson et al., 2012), to an advectively and atmospherically controlled thermocline in the west (Largier & Swart, 1987), where it is further from the influence of the Agulhas Current and closer to the strong upwelling winds of the Benguela upwelling system. Thus, temperature on the Agulhas Bank is controlled by a combination of wind-driven coastal upwelling and current-driven shelf edge upwelling (Beckley, 1983; Goschen et al., 2012; Lutjeharms, 2006; Lutjeharms et al., 2000).

In the last decade, much of the work on the Agulhas Bank has focused on a population shift of the commercially important *Sardinops Sagax* (sardine) and *Engraulis encrasicolus* (anchovy) eastward from the west coast to the Eastern Agulhas Bank. There are three hypotheses for this shift: (i) intense fishing pressure on the west coast, (ii) an environmentally induced shift, and (iii) an increase in spawning success in the eastern population (Coetzee et al., 2008). Roy et al. (2007) explored the environmental shift hypothesis for the abrupt eastward shift in distribution, which occurred in 1996. The eastward shift in anchovy distribution coincided with a temperature drop of 0.5 °C on the inner shelf to the east of Cape Agulhas (20°E), which was ascribed to a change in zonal wind stress forcing.

Due to the limited temporal coverage of satellite sea surface temperature (SST) data, possible environmental shifts on the Agulhas Bank have not been explored on longer time scales and the dynamics of upwelling

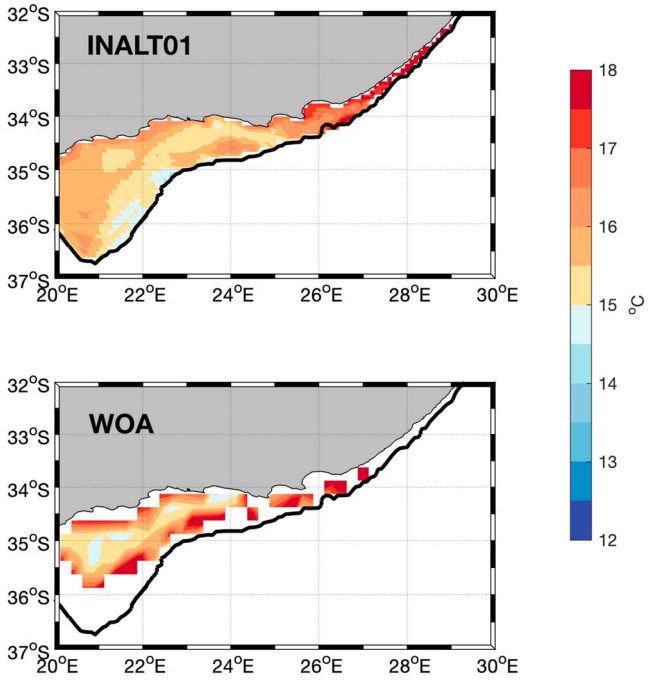

Figure 1. Depth-averaged mean temperature (°C) calculated from 1948 to 2007 for areas <200 m in depth on the central and eastern Agulhas Bank from INALT01 (top) and World Ocean Atlas observations (bottom); the black solid line shows the 200-m isobath.

processes are not well understood. This lack of understanding of the decadal variability presents a challenge for management decisions, particularly in the realm of Marine Protected Areas and fisheries resources. Added to this, the long-term ocean observational record in this area is limited in the face of the complexity and dynamic nature of the region (Morris et al., 2017), making it necessary to explore alternate methods of understanding the long scale variability of the Agulhas Bank. Here the ability of an ocean general circulation model (OGCM) developed for the Agulhas System and forced by atmospheric reanalyses to resolve the 1996 environmental shift, highlighted by Coetzee et al. (2008) and Roy et al. (2007), is investigated, and the interannual to decadal variability of water temperatures on the Agulhas Bank is examined for the period 1948–2007. Use of OGCM output in undersampled areas of the ocean facilitates the analysis of ocean state variables with depth. This includes changes in deeper temperatures and currents and their relationship with spawning and population distribution, which are not accounted for in studies using surface data only.

This is especially notable in light of observed mismatches between surface temperature, chlorophyll concentrations, and actual copepod and pelagic biomass distributions in this shelf region to the east of 18°E (Grémillet et al., 2008). It also allows a longer time period to be investigated, as spatially and temporally consistent observations are only available for the satellite era (1979 onward). This work seeks to uses an OGCM to explore an influential environmental shift in temperature over the Agulhas Bank discussed by Roy et al. (2007). The OGCM is then used to investigate any similar shifts in previous decades and diagnose the large-scale patterns controlling temperatures in the shelf waters over decadal time scales. It must be noted that, in order to run experiments over the long time period considered here, it is necessary to make a trade-off between the length of the model run and the resolution of the atmospheric forcing available. For this work, with its focus on multidecadal variability, it was chosen to prioritize the length of the model run, and so use lower resolution forcing, which may result in some synoptic-scale variability not being resolved.

2. Data and Methods

2.1. Model Output

INALT01 is a high-resolution nest within a global coarse-resolution ocean/sea ice configuration (Durgadoo et al., 2013), based on the Nucleus for European Modeling of the Ocean (Madec, 2008). The (1/10)° domain is 8°N to 50°S, 70°W to 70°E, two-way nested into the global (1/2)° grid using a two-way nesting approach (Debreu & Blayo, 2008). There are 46 vertical layers in z coordinates, 10 of which are in the top

Table 1
Summary of Wind Products

Product	Time period	Spatial resolution	Data type
CORE	1948–2008	2°	Reanalysis
NCEP1	1948 to present	2.5°	Reanalysis
ERA-interim	1979 to present	0.7°	Reanalysis
CCMP	1987 to present	0.25°	Merged observations

Note. NCEP = National Center for Environmental Prediction; CCMP = Cross-Calibrated Multi-Platform.

100 m, and the deepest grid cell is allowed to be partially filled (Barnier et al., 2006), improving the interaction of near-bottom flows with the topography. Lateral momentum boundary conditions are free slip. Bathymetry from the 2-min resolution Gridded Global Relief Data (ETOPO2v2) is interpolated onto the nested model grid.

INALT01 is forced using COREv2b (Large & Yeager, 2009) atmospheric and flux fields originally derived from the 60-year time series of the National Center for Environmental Prediction and National Center for Atmospheric Research reanalysis project (from here on NCEP1; Kalnay et al., 1996) interpolated onto the model grid from its original 2° × 2° resolution. Two runs of INALT01 are used in this study, both starting from the same initial conditions, the first using interannual forcing from 1948 to 2007 and the second using climatological, repeated-year forcing for 60 years. Both 5-day and monthly mean output are used, and model drift has been removed using the linear trend from the climatological run. As both experiments are run from the same starting point, any trend in the repeat year climatological forcing experiment can be assumed to be caused by numerical model drift, which will also be present in the interannually forced run (similar to Durgadoo et al., 2013). Use of CORE as a forcing data set, while coarse in spatial resolution for a shelf application, and thus not suited to the event scale, allows a long enough time series for the decadal scale to be considered, unlike in models using higher resolution forcing such as ERA-interim reanalysis or observed scatterometer winds.

In order to examine and summarize decadal temperature variability on the shelf as a whole, temperature is averaged from the surface to the bottom, and only the area with water depth less than 200 m is considered. This accounts for both surface and subsurface temperature changes, as in the case of marine heat waves the maximum intensity of warming has been shown to be subsurface (Schaeffer & Roughan, 2017). From here on this is referred to as shelf temperature.

Although a depth-averaged temperature field does not take into account mixed layer and thermocline depth dynamics, it does provide a simple robust metric with which to assess temperature mean changes across different dynamical regimes in different water depths and shelf configurations, such as the eastern and western Agulhas Bank. Use of more targeted metrics, for example, mixed layer depth or choice of a certain depth level, is more sensitive to high-frequency dynamics and aliasing and therefore more subjective at the decadal time scales which are the focus of this study.

The temperature in the top-most model grid box is tied through bulk formulation to the atmospheric forcing. In order to avoid any bias in averaging, we omit the upper box. The mean of the resulting shelf temperature and a comparison with observations from World Ocean Atlas (Conkright et al., 1994) is shown in Figure 1.

2.2. Wind Data

There are two primary physical mechanisms by which the wind can control ocean temperatures on the shelf. The first is the creation of surface convergence or divergence as a result of Ekman transport; this can be either coastal divergence or Ekman pumping in the open ocean. The second is via changes in the amount of wind-driven vertical mixing, and contributions may also be made by changes in wind-driven component of evaporative cooling. Surface winds from two atmospheric reanalyses and one observed wind product were used. The COREv2b (Large & Yeager, 2009) forcing covers the period 1948 to 2008. The ERA-interim reanalysis Dee et al. (2011) covers the period 1979 to present. As an observationally based wind product, the Cross-Calibrated Multi-Platform (CCMP) 10-m winds (Atlas et al., 2011) are used. This is a (1/4)° resolution, global, 6-hourly vector wind product, which uses variational analysis to combine multiple cross-calibrated

satellite scatterometer data sets with in situ measurements. The wind data sets used and their properties are listed in table 1.

Here following Bravo et al. (2016), Ekman transport Ek (m^2/s) is calculated as follows:

$$Ek = \frac{1}{\rho_{wf}} \tau \times k \quad (1)$$

with ρ_w representing the water density (taken as 1,025 kg/m^3), f the Coriolis parameter, τ the alongshore (in this case zonal) wind stress, and k a vertical unit vector. The wind stress (N/m^2) is calculated as follows:

$$\tau = \rho_a C_d |v| v \quad (2)$$

with the density of air ρ_a at 1.2 kg/m^3 and the drag coefficient C_d as 0.0013 as per Smith (1988). Drag is assumed to be constant, and the influence of changing wind speed and vertical heat fluxes on the drag coefficient is assumed to be unimportant. As the bulk of the coastline from 20°E to 26°E is approximately zonal due to the shape of the embayments, zonal winds are taken to be alongshore to enable more objective comparison across wind products of differing resolutions.

NCEP1 (Kalnay et al., 1996), which forms the primary atmospheric input of the CORE forcing fields, is one of few attempts to analyze the state of the global atmosphere for a period of longer then 50 years. The length of the available time series (60 years is used here) enables the exploration of decadal and multidecadal cycles in the forcing of the ocean. However, as the NCEP1 reanalysis ingests all available data since 1948 for its data assimilation, it is to some extent dependent on the density and quality of available observations. With the expansion of the global observation network from 1948 to the present day, and particularly the global coverage provided in the satellite era, there are changes, in both time and space, of the relative weighting of the model forecasts and observations to the final solution. This issue is well known and has been investigated in a number of studies (Chelliah & Ropelewski, 2000; Kistler et al., 2001; Powell & Xu, 2011; Sturaro, 2003).

Considering winds in particular, Wu and Xie (2003) found equatorial Pacific surface wind changes around 1977, from the reanalysis product, to be at odds with those in the Comprehensive Ocean-Atmosphere Data Set observations. Thus, this reanalysis is not considered appropriate for the detection of global climate change (Chelliah & Ropelewski, 2000) but can provide powerful tools for studies at the regional scale which present strong climate signals (Sturaro, 2003).

It must be noted that there are known issues with the high-latitude Southern Hemisphere pressure fields in the presatellite years before 1979, due to a lack of observations (Hines et al., 2000; Kistler et al., 2001; Sturaro, 2003). However, the area considered here is located near 34–37°S where these biases are less marked. Hill et al. (2008) note this and use NCEP1 winds in a similar study of multidecadal variability in the East Australia Current. Additionally, in order to minimize the effect of these biases, NCEP is compared against independent data sets where possible, and the station observation derived Southern Annular Mode (SAM) index of Marshall (2003) is used, rather than the an NCEP derived SAM index, which would be strongly affected by high-latitude biases in sea level pressure.

3. Results

3.1. Shelf Temperatures

A time series of INALT01 shelf temperatures between 20°E, where the Agulhas Bank is at its greatest extent, and 27°E, the easternmost extent of the Bank, is plotted for the years from 1948 to 2008 (Figure 2). Although there is a large amount of high-frequency variability in the temperature fields over the Agulhas Bank due to weather systems, mainly cold fronts, cutoff lows, ridging anticyclones and cloud bands (Weldon & Reason, 2014), and the influence of the Agulhas Current, the use of a Hanning filter, with a 2-year window to remove seasonal and subseasonal variability, reveals considerable interannual and decadal variability. This filtered time series shows two striking shifts occurring in the temperature of Agulhas Bank shelf waters during the 60-year time series. The first of these large temperature shifts occurs in 1966, where the mean shelf temperature warms from 21 to 21.82 °C. These warmer temperatures are maintained for the next three decades until a 0.8 °C drop in shelf temperatures occurred in 1995–1996. These shifts in temperature of approximately 1 °C occur over a timespan of less than 2 years and enable the 1948–2008 time period to be separated into three distinct segments (shown in differing colors in Figure 2); a cold period from 1948 to 1966, a warm period from 1967 to 1996, then reverting to a cool period from 1997 to 2008. The cooling in the

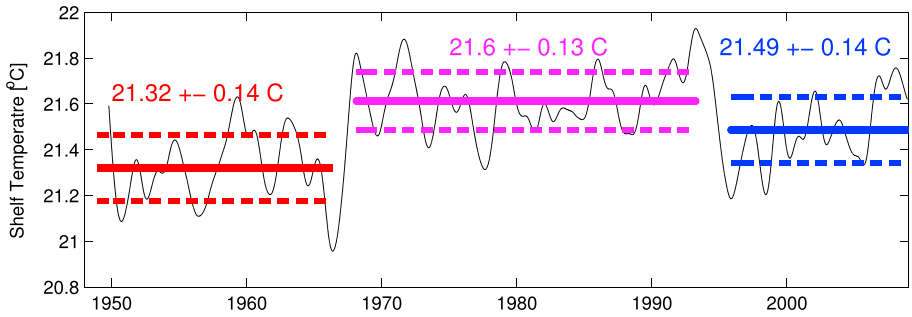

Figure 2. Simulated depth-averaged temperature for Agulhas Bank waters shallower than 200 m between 20°E and 27°E. Filtered 5-daily output is shown by the thin black line, with the three periods representing cold and warm regimes shown in color.

mid 1990s is consistent with the environmental shift observed by Roy et al. (2007) and discussed in Coetzee et al. (2008).

Climatic regime shifts are commonly detected and tested for significance using a paired Student's *T* test, assuming a normal distribution and equality of variances (Rodionov, 2005). Here we apply a paired-sample Student's *T* test and find that both shifts (1966 and 1996) are significant at a 99% significance level. There is no significant change in the variance over the time series, and the trend from 1948 to 2007 is not significant. These assumptions were confirmed by performing a Welch's *T* test, which produced the same results as the Student's *T* test.

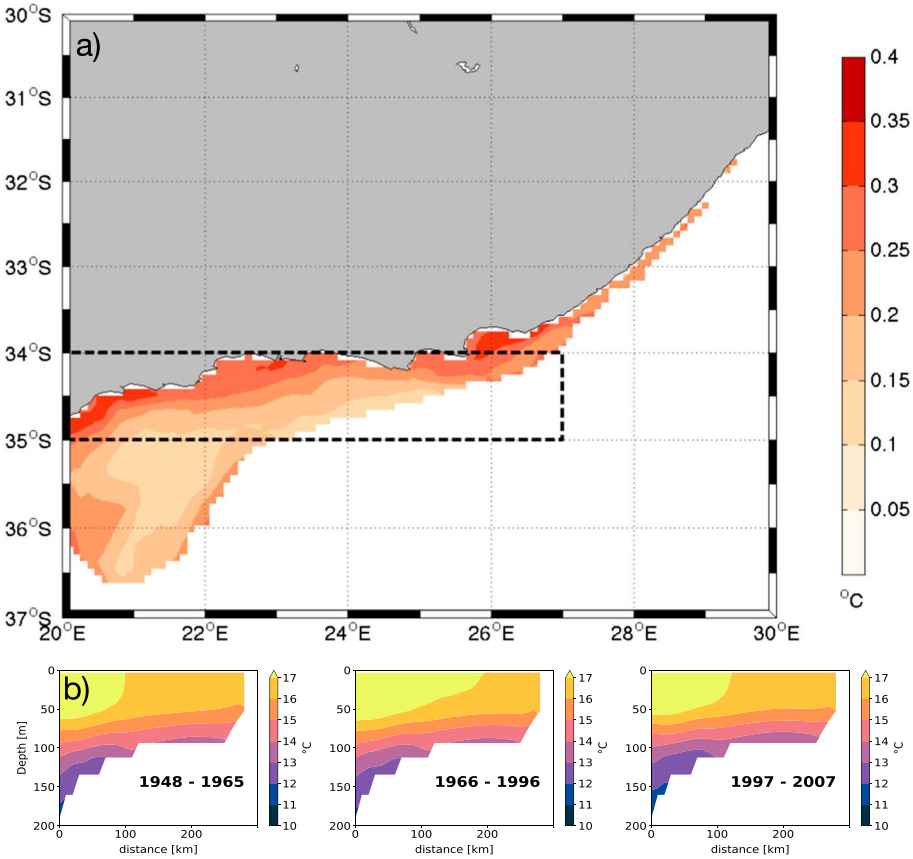

Figure 3. (a) Difference between depth-averaged temperatures (°C) for the Agulhas shelf region between cold regimes (1948–1966 and post-1996) and warm regime (1967–1995). The first grid points extracted for the time series in Figure 5 fall within the dashed black box. (b) Sections of model temperature at 21°E, averaged for each time period.

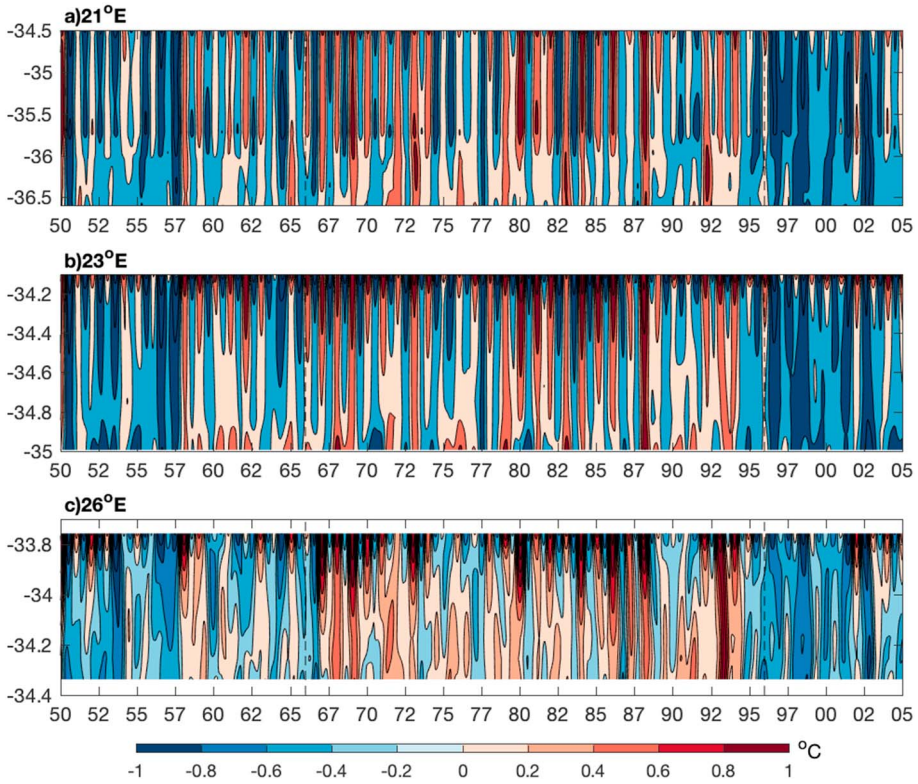

Figure 4. Hovmoller latitude-time plot of simulated shelf temperature anomaly (°C) at 21°E (a), 23°E (b), and 26°E (c). Light vertical dashed lines show the years 1966 and 1996.

The spatial distribution of shelf temperature shows distinct differences between the composite mean of the cold regimes (pre-1966 and post-1996) and the warm regime (1967 to 1995) of Agulhas shelf waters in INALT01 (Figure 3a). The positive shelf temperature anomalies are strongest (in the order of 0.3 °C) in shallower waters along the coast between 20°E and 27°E, with the largest area of warming extending close to the entire shelf width at 26°E off Algoa Bay. As the shelf widens to the west, the warming remains focused along the coast, while the midshelf and shelf edge warming is small.

This concentration of warming along the coastline suggests that changes in wind-driven coastal upwelling and downwelling as the most likely driver of multidecadal shelf temperature shift over the Agulhas Bank. Most strong warming occurs within one baroclinic Rossby radius of the coastline (approximately 30 km; Chelton et al., 1998) indicating that upwelling is driven by divergence at the coast, or the coastward movement of warm Agulhas Current surface water via Ekman transport rather than open ocean upwelling from Ekman pumping. Variability forced by large-scale changes in atmospheric temperature,or shifts in the Agulhas Current itself, would also express itself more equally over the bank and have a strong warming effect on the narrow shelf east of 27°E, pointing to coastal winds as the primary forcing mechanism of coastal warming. Sections of temperature taken at 21°E, where the shelf is widest, show the notable movement of the surface outcrop of the 17 °C isotherm between the warm and cool periods (Figure 3b). In the cool period from 1948 to 1965, the 17 °C isotherm lies approximately 100 km from the 200-m isobath. In the warm period 1966 to 1996, the 17 °C isotherm moves shoreward almost 100 km, to lie 200 km inshore of the 200-m isobath, while in the second cool period, 1997 to 2007, it retreats back offshore to around 120 km from the 200-m isobath. This movement of the 17 °C isotherm, along with a slight raising and lowering of the 16 °C isotherm are the dominant signal between the cold and warm periods, while the changes offshore and at depth are relatively small, with there being a small increase in the intrusion of cold water up the shelf from 200 to 100 m in in 1997 to 2007 period.

Considering the nature of this warming across the shelf over time at three longitudes, 21°E, 23°E, and 26°E, reveals more detail of the warm regime from the mid-1960s to the mid-1990s (Figure 4). Despite the removal of the seasonal cycle and the application of a 73-point Hanning filter in time, there is still considerable inter-

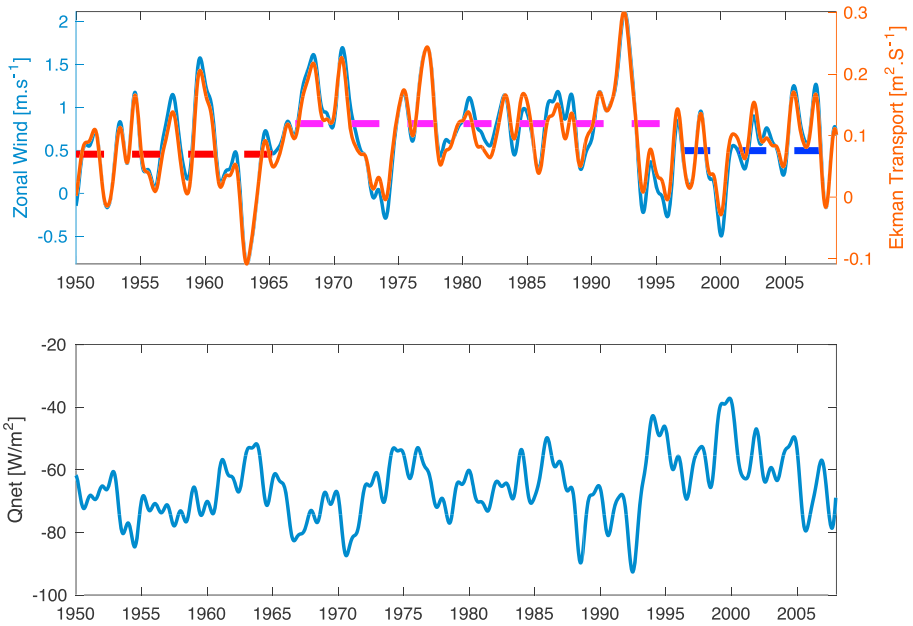

Figure 5. (top) Zonal CORE winds (+ve is eastward and therefore downwelling) and Ekman transport (+ve is northward) for coastal Agulhas Bank (34–35°S, 20°E to 27°E), the colored dashed lines indicate the three different regimes. (bottom) INALT net downward heat flux (5-day means, smoothed with a 2-year filter, negative values show transfer of heat from ocean to atmosphere).

annual variability, much of which is likely to the be forced by the strong influence of the Agulhas Current on these shelf waters. At 21°E, where the shelf is at its widest, a predominance of colder years, with temperatures 1 °C below the mean, are seen between 1950 and 1960. In the 1960s, small warm events, with positive anomalies of 0.5 °C, increasing to 1 °C, are seen but confined almost exclusively to a very narrow region along the coastline. These warm events grow stronger and increase their offshore extent in the ensuing years, until 1996 where a general pattern of cold events, more than 0.5 °C below the mean, sets in, although some small, sporadic coastal warm events are seen.

A similar pattern of of coastal warm events for a 30-year period is seen at 23°E, where the shelf is approximately half of the width. Here, the 1 °C coastal warming events are more consistent throughout the "warm decades" of the 1960s, 1970s, and 1980s and have a larger offshore extent. The pattern continues in the narrow shelf off Algoa Bay at 26°E, although the warming is less marked here.

3.2. Multidecadal Wind Variability

To explore wind-driven upwelling as a potential driver of the temperature regime change over the Agulhas Bank, the zonal winds from CORE and their resulting onshore Ekman transport have been averaged over a coastal box encompassing the closest grid point to the coastline (34–35°S, 20°E to 27°E, Figure 5). Although these coastal winds are downwelling in the mean, downwelling component winds are noticeably stronger in the period 1966 to 1994 when compared to the periods before and after, matching the regime changes in depth-averaged temperature seen in Figure 2. For the 1948–2008 time period there is a significant correlation ($r = 0.63 p = 0.001$) between the 2-year smoothed zonal coastal winds and depth-averaged shelf temperature between 20°E and 27°E. The same Welch's T test performed on the zonal winds as was performed on the shelf temperatures reveals that there are significant shifts (at a 95% significance level) in the zonal wind regime in this coastal box in 1966 and 1996.

To get an idea of the effect of the change in wind-driven heat transport caused by these shifts in zonal winds, a simple scaling exercise can be done to estimate the Ekman heat transport following the method of Sprintall and Liu (2005) where the Ekman heat flux is given by

$$\Theta^{y}_{Ek} = -c_p \int_{x2}^{x1} \frac{\tau_x}{f}(\theta_e - \bar{\theta})\mathrm{d}x \tag{3}$$

where c_p is the specific heat capacity of water (assumed constant and equal to 4000 J·kg^{-1}·°C^{-1}), θ_e is the Ekman layer potential temperature (estimated from sections in Figure 3 to be 17 °C), and $\bar{\theta}$ is the mean

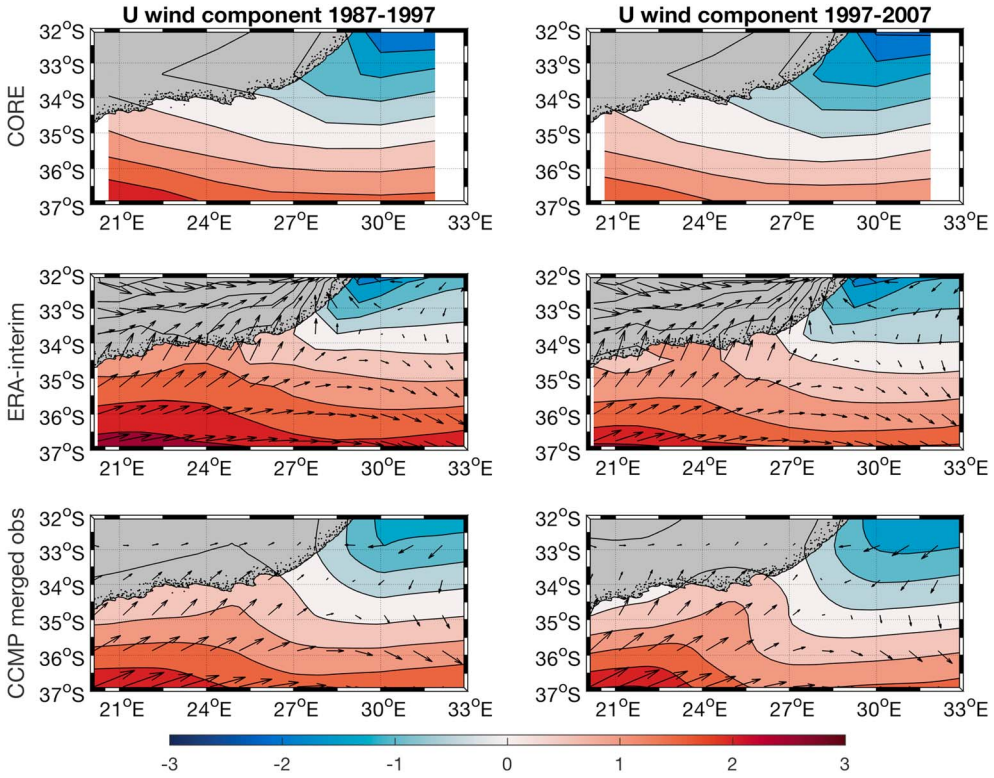

Figure 6. Zonal wind component (colors, m/s) for CORE (top row), ERA-interim (middle row), and CCMP (bottom row) for the decades 1987–1997 (left column) and 1997–2007 (right column). +ve shading shows westerly component (downwelling) winds, and -ve shading shows easterly component (upwelling) winds. Wind vectors are shown for the two higher-resolution data sets. CCMP = Cross-Calibrated Multi-Platform.

temperature of the water column (estimated from sections to be 14 °C). The zonal component of the wind stress is taken from the calculation of Figure 5, as 0.005 N/m^2 during the cold periods and 0.01 N/m^2 during the warm period. Integrated over a 1-m^2 water column, this gives an Ekman heat flux of 74 W/m when using a wind stress typical of the cold periods and 148 W/m during the warm (i.e., 1966–1996) period. It is notable that the pivot years between the regimes (i.e., mid-1960s and mid-1990s), where large step changes in shelf temperatures occur, coincide with the 2-year maximums and minimums of Ekman heat transport.

The possible role of changing downward heat flux from the atmosphere must also be taken into account, especially considering that the warm period between 1966 and 1997 is most apparent in shallow waters along the coast, which will be more affected by changes in heat in the surface boundary layer with the atmosphere. The bottom panel of Figure 5 shows the net downward heat flux from INALT01 for the same area as the zonal winds above. While the interannual variability in heatflux is considerable, especially in the early 1990s, the correlation between downward net heat flux and shelf temperature is not significant ($r = -0.32, p = 0.001$). In order to test the robustness of these multidecadal shifts in zonal winds, the 1996 regime change is used as a case study. As this shift falls within the satellite era, it is possible to compare zonal wind fields from CORE to the higher resolution ERA-interim reanalyses and the CCMP merged observational data set (Figure 6). In both decades, all three data sets show a transition from annual mean downwelling (westerly) winds to the south and annual mean upwelling (easterly) winds to the north. This transition manifests itself as a southward movement of the zero line between westerly and easterly component mean winds. In CORE, the zero line between easterly and westerly mean winds migrates 0.5° southward to the east of 26°E and 1° southward to the west of 26°E, in the area shown by Figure 3 to have warmed in the previous regime shift and thus can be hypothesized to be most sensitive to changes in wind-driven upwelling. This pattern of a southward shift of the zero line in zonal wind stress is mirrored in both the ERA-interim and CCMP data sets, with a stronger expression in the observed CCMP data set than in the two reanalysis products.

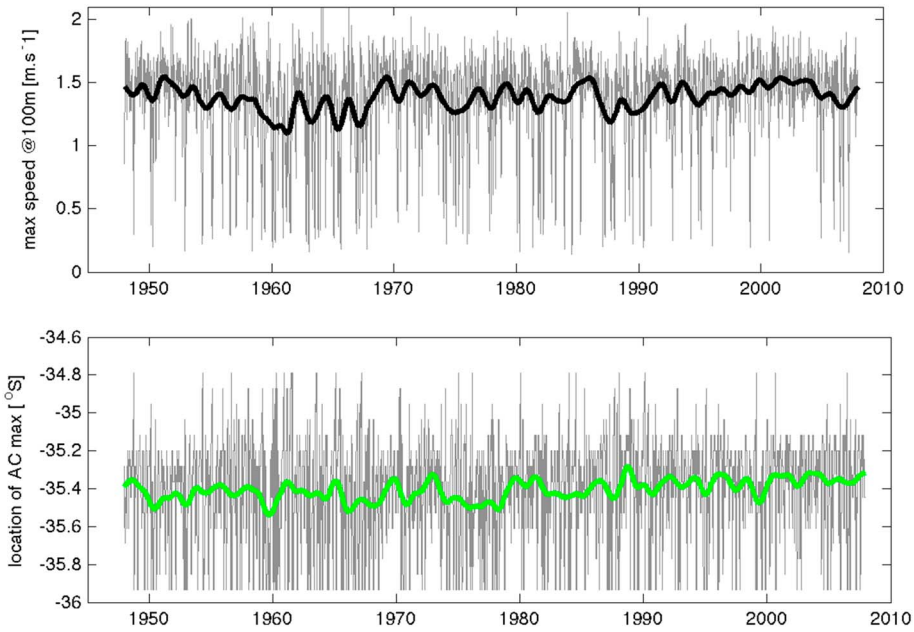

Figure 7. Maximum current speed at 100 m from INALT01 at 24°E (top) and latitudinal position of that maximum (bottom); thicker lines are filtered with 2-year Hanning filter.

3.3. Agulhas Current Variability

To examine whether changes in the position or strength of the Agulhas Current's dynamical core may have contributed to regime changes in temperature on the Agulhas Bank, the velocity structure at 100 m was considered. Figure 7 shows the intensity and position of the Agulhas Current's core at 24°E. A depth of 100 m was chosen in order to minimize the impact of the wind-driven component of the flow. To generate the time series, using a modification of the method established in Malan et al. (2018), the intensity of the current is taken to be the maximum scalar speed at 100 m along the longitude of 24° E between 34°S and 36°S. Both the position and speed show considerable interannual variability, but not the significant multidecadal variability seen in both temperature and zonal wind stress. The largest decadal shifts in intensity take place in the late 1960s and the late 1980s but are far smaller then the shifts seen in temperature and wind stress, while position shows interannual, but little decadal variability. A summary of the correlation of zonal wind stress, net downward heat flux, Agulhas Current position, and Agulhas Current strength with the shelf temperature time series in show in Table 2. Correlations are calculated with a 2-year hanning filter and 30 degrees of freedom.

3.4. Effects of Interannually Varying Winds

In order to confirm the role played by interannual and multidecadal zonal wind variability on the shelf water temperature of the Agulhas Bank, the depth-averaged shelf temperature as shown in Figure 2 was also calculated for a 60-year run of INALT01 using repeat climatological forcing rather than interannually varying forcing. The shelf temperatures for the 60 years of each run are compared in Figure 8. It is immediately apparent that, when running the model with repeat year climatological forcing, and thus removing the effect of the north-south migration of the wind belts, the striking shifts in shelf temperature taking place from the mid-1950s to mid-1960s and from the late-1980s to mid-1990s are no longer apparent. Interannual variability is still seen in both the climatological and interannual simulations as a result of internal variabil-

Table 2
Summary of Correlation of Drivers of Shelf Temperature

$p = 0.001$	TauX	Qnet	AC position	AC strength
r	0.63	−0.32	0.13	0.15
significant	yes	no	no	no

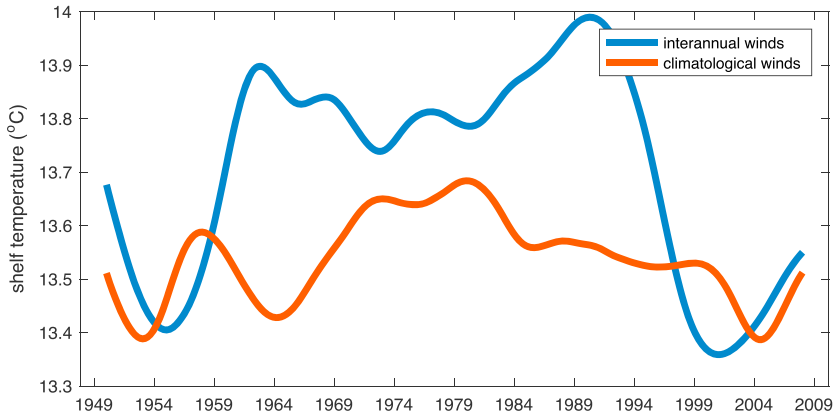

Figure 8. Monthly means of simulated depth-averaged shelf temperature from INALT01 runs with both interannual and repeat year climatological forcing. Model drift was accounted for by calculating the linear trend from the climatological experiment and removing it from both the interannual and climatological time series which are then filtered with a 10-year low-pass Hanning filter.

ity in the Agulhas Current itself, but the marked shifts in mid-1960s and mid-1990s appear to mainly be a function of the interannual wind forcing alone.

3.5. Large-Scale Context of Multidecadal Wind Shifts Off Southern Africa

The latitudinal migration of the zero line between an easterly mean wind and a westerly mean wind over the south coast of South Africa is related to larger, hemispheric scale changes in pressure systems. In order to increase the length of the available time series in the observation-rich satellite era, the NCEP1 winds have been used rather than CORE (NCEP1 and CORE correlate with $r = 0.9$). A composite anomaly of sea level pressure from NCEP for the 1966 to 1996 period (Figure 9) shows large area of negative pressure anomaly to the southeast of southern Africa, centered on 43°S, 45°E, as well as positive pressure anomalies further south in the westerly wind band. It is plausible that the additional cyclonic circulation driven by the low-pressure anomaly has resulted in the greater westerly component in the coastal Agulhas Bank winds seen in Figure 5 and thus in the warm period from 1966 to 1997 seen in Figure 2. Alternatively, shifts in the north-south extent of the South Atlantic High could act to allow more cold fronts to impact on the south coast of South Africa, bringing an increase in the number of days with westerly component downwelling winds. The negative sea level pressure (SLP) anomaly centered on 35°S, 0°E appears to support this idea, but it is difficult to draw conclusions due to the unreliable nature of NCEP SLP fields in this early period. It should be noted that anomalies shown in Figure 9 are calculated from the recommended climate normals of the period 1981–2010, as suggested for placing climate conditions into a historical context (Arguez et al., 2012). However, the uncertainty in the early part of the period considered here makes the choice of climatological period extremely subjective. Thus, the approach taken is to identify broad patterns and then verify them against more reliable, station-based indices.

The large-scale pattern of positive sea level pressure anomalies in the high latitudes of the Southern Ocean and negative anomalies north of about 45°S seen in the NCEP SLP of Figure 9 is consistent with a negative phase of the SAM. Considering the sea level pressure at the hemispheric scale, the pattern south of 60°S is consistent with a negative phase of SAM. The midlatitude pattern is more subtle than a classical SAM, with strong low-pressure anomalies only present at 45°S to the southeast of southern Africa as well as the east of South America. The pattern is reminiscent of the zonal wave 3 pattern (Raphael, 2004), which has been associated with influencing the tracks of midlatitude storms. Despite the possible complexity, the presence of a SAM-like pattern suggests that the shifts in the large-scale circulation responsible for the temperature regime change on the Agulhas Bank is consistent with a negative phase of SAM and its associated increase in midlatitude westerlies (Marshall, 2003). Negative phase SAM is associated with more midlatitude storms and westerly flow affecting the southern part of South Africa (Reason & Rouault, 2005). An increase in midlatitude westerlies results in a northward shift in the zero line from mean westerly to mean easterly winds (Figure 6) and thus increased downwelling along the coastal Agulhas Bank. Although this shift in the zero line is small (order 1° of latitude), it crucially is located directly over the southern coast of South Africa.

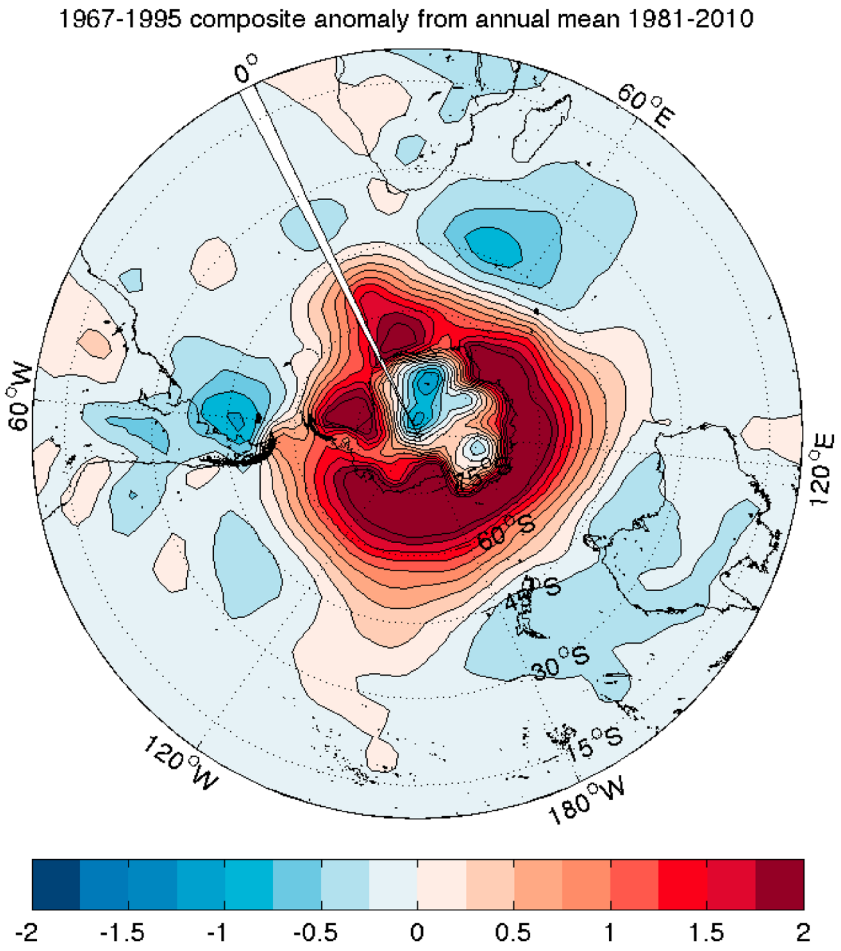

Figure 9. Composite anomaly of sea level pressure for the years 1966 to 1996 calculated off the 1981 to 2010 climatology.

In order to confirm this relationship against a more reliable, station-based index, NCEP zonal wind stress anomalies over the Agulhas Bank are correlated with the monthly observed SAM index (Figure 10, as defined by Marshall, 2003, for the full available time series of the SAM [1957–2016]; Figure 11). SAM and zonal wind stress correlate significantly ($r = 0.4$, $p = 0.1$) along the South Africa south coast. Thus, a negative SAM coincides with stronger downwelling winds on the SouthAfrican south coast.

4. Discussion

The INALT01 model simulation shows a significant shift in temperature in the water column of the Agulhas Bank, which is consistent with that reported from satellite observations by Roy et al. (2007). The shift in the mid-1990s from a warm regime to a cold regime is statistically significant and driven by a slight southward shift in the zero line between the annual mean westerly component winds to the south of the south coast of South Africa, which is oriented zonally at approximately 34°S and mean easterly components to the north.

Interestingly, the model also shows an earlier, and stronger, regime shift in the mid-1960s. Unfortunately, acoustic surveys for spawner biomass of anchovy and sardine only began in 1984, so little attention has been given to this earlier environmental shift and whether it shows the same relationship to small pelagic population distribution as the shift in the mid-1990s. However, a sharp decline in sardine catches in St. Helena Bay on the west coast of South Africa, from 400 million to 100 million tons between 1964 and 1966 was reported by Verheye et al. (1998).

The ability of INALT01 at a (1/10)° resolution, forced by the coarse-resolution (2° resolution) CORE fields, indicates that to the first order the mechanism controlling shelf temperatures on the central and inner Agulhas Bank is a relatively straightforward one. The warmer shelf waters simulated between 1966 and 1996

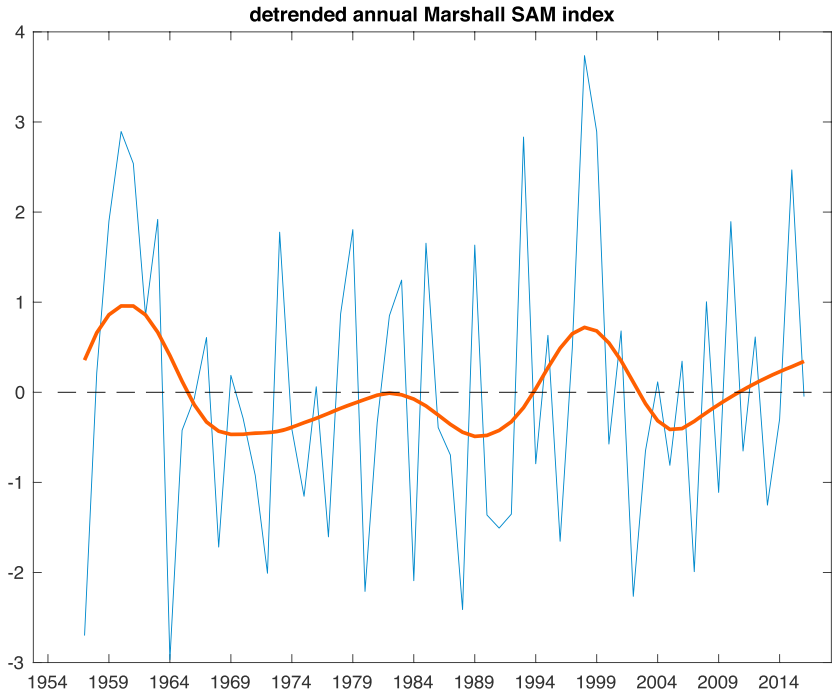

Figure 10. Annual values of the Southern Annular Mode Index (Marshall, 2003); the orange line is filtered with a 20-year window.

show their most intense warming along the coastline rather than in the midshelf. This suggests that these warmer temperatures are driven by an increased Ekman transport toward the coast, resulting in an increase in downwelling of warm surface water; this is further supported by most warming being confined to within the baroclinic Rossby radius of the coast. This mechanism of the warm period from 1966 to 1996 being by an increase in downwelling winds is confirmed by comparing the absence of this warm period in a model run with climatological wind forcing. It should be noted that the use of climatological forcing also removed the large step changes in the sign of the temperature anomaly temperature that happen in the years immediately before and after a regime change. That shelf temperatures are sensitive to relatively small changes in the large-scale winds; that is, changes in the wind fields that are not large enough to affect the Agulhas Current itself, is particularly interesting. This sensitivity of the shelf temperatures to the north-south movement of the zero line between mean westerly and mean easterly zonal winds is attributed to the zonal orientation of the coastline, and it being situated on the boundary between these westerly and easterly wind regimes.

It is notable that the regime shift is not stronger in a particular season or month than it is when considering the full data set. This can be attributed to the effect of large meander events in the Agulhas Current, which have been shown to affect the circulation of the Agulhas Bank an average of 110 days per year (Krug et al., 2014) and can drive temperature anomalies as large as the seasonal cycle (Malan et al., 2018). As these meanders are such a strong driver of temperature anomalies but are created by nonlinear processes and so do not show seasonality, a meander can cause a few months of a year to have highly anomalous temperatures, although the year itself may not be unusual. Thus, while meanders can cause considerable intra-annual and interannual variability in shelf temperature, especially when combined with anomalously high upwelling winds such as documented in the Gulf Stream by Hyun and He (2010), over the decadal time scales considered here, their effect is canceled out.

There does not appear to be any relationship between the warm regime from 1966 to 1996 and a change in the position or strength of the Agulhas Current and the relationship between shelf temperature and net downward heat flux, while undoubtedly having an effect on surface temperatures, does not show a significant correlation with shelf temperature. However, the increase in the flux of heat from the atmosphere into the ocean over the last 60 years supplies a possible explanation for the regime shift in 1996 being smaller in magnitude than that of 1966. Thus, surprisingly, despite the Agulhas Bank being strongly influenced by the presence of the highly dynamic inshore front of the Agulhas Current, which dominates the variabil-

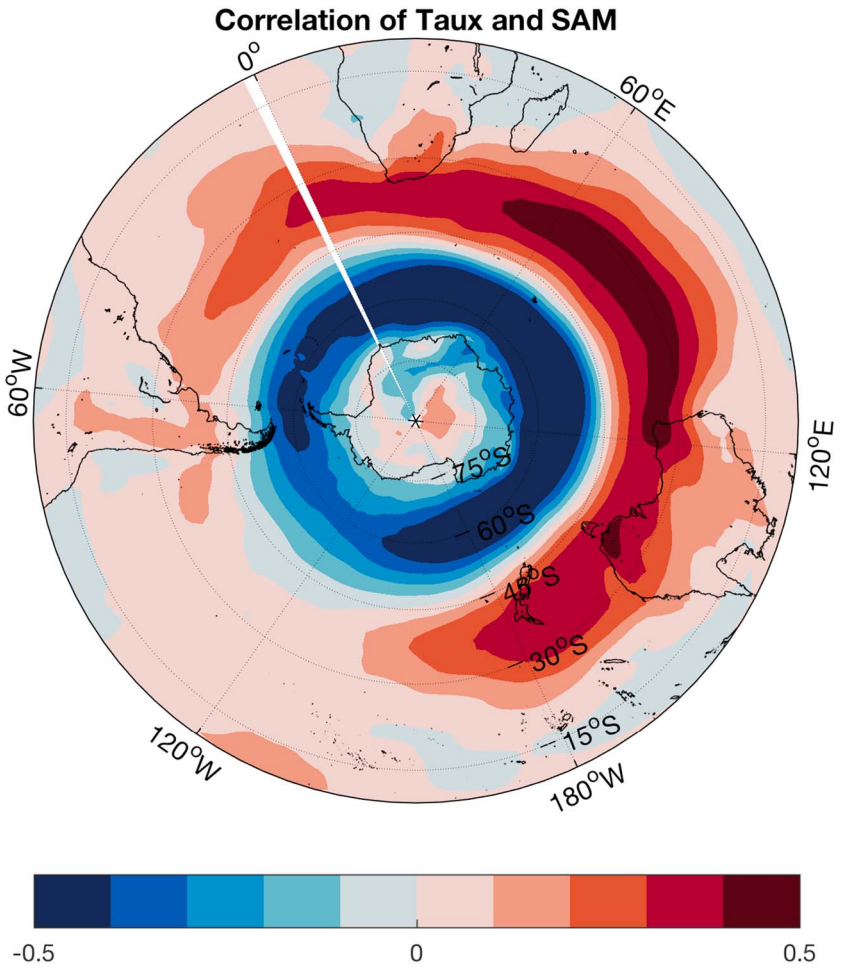

Figure 11. correlation of National Center for Environmental Prediction zonal wind stress anomalies with the monthly Marshall Southern Annular Mode (SAM) index, 1957 to 2016 (both detrended, $p = 0.1$).

ity on subseasonal temporal scales, the decadal variability in temperature is dominated by the coastal wind field. This is especially surprising on the narrow shelf east of 24°E, which is known to have strong dynamic upwelling driven by the Agulhas Current (Leber et al., 2016; Lutjeharms et al., 2000). This highlights the complexity of the upwelling mechanisms at the shelf edge off Algoa Bay (Goschen et al., 2012) and the role of wind-driven processes in outcropping upwelled water to the surface or advecting warm surface water coastward from the Agulhas Current.

The relationship between SAM and the coastal upwelling on the Agulhas Bank is an encouraging one in terms of the predictability of the physical environment of the Agulhas Bank as a tool for the management of resources. However, the possible biases of reanalysis products in the presatellite era, as well as the short time series (in multidecadal terms) available, mean that a high-resolution coupled ocean and atmosphere model experiment would be needed to explore the exact dynamics involved in the connection of the large-scale atmospheric circulation to the coastal wind changes. This is highlighted by the fact that while correlations between the observational SAM index and coastal zonal winds (both monthly means) from NCEP (Figure 11), the same analysis performed on a reanalysis-derived SAM index is not significant, due to the large difference between observed and reanalysis winds in the Southern Ocean in the presatellite era. Thus, while this correlation is encouraging, a long enough time series is (either observational, or using a model forced by a realistic atmosphere) not available to give any certainty of this relationship, as here only one or two cycles of the Agulhas Bank regime shift are resolved.

An increased understanding of these dynamics would open up the possibility of some predictive skill in anticipating temperature regime changes on the Agulhas Bank driven by large-scale shifts in the zonal wind

patterns. This study shows that use of an ocean model of a similar resolution to the next generation of climate models allows this process to be understood, thus allowing global change scenario planning for the South African south coast to be carried out in the near future.

Use of long time series from reanalysis products is important in order to place the observations from the satellite era into a longer term context. Studies of trends in SST (Rouault et al., 2009, 2010) show a decreasing trend of coastal SST on the south coast of up to 0.4 °C per decade from 1982 to 2009 using the optimally interpolated observed SST product from Reynolds et al. (2002). The evidence from the OGCM simulation presented in this study suggests that these trends in SST may rather be the result of the system shifting from one regime to the other or returning to equilibrium from an abnormally warm state. This demonstrates the importance of the use of numerical ocean models, in conjunction with observational programs, in placing what we observe in the real ocean into a greater dynamical context.

Acknowledgments
INALT01 was developed at GEOMAR, with details of its configuration and access to data available at https://www.geomar.de/en/research/fb1/fb1-od/ocean-models/inalt01/. COREV2b data were accessed at the RDA (www.rda.ucar.edu/datasets/ds260.2/), NCEP data were accessed at the www.esrl.noaa.gov/psd/data/reanalysis/reanalysis.shtml website, ERA-interim data were accessed at http://apps.ecmwf.int website, and CCMP was accessed at the website (podaac.jpl.nasa.gov/Cross-Calibrated_Multi-Platform_OceanSurfaceWindVectorAnalyses). We would like to that the two reviewers for their time and input, which has added considerably to the quality of this paper. This work was funded by the Professional Development Programme of the DST managed by the NRF-RISA and the Nansen-Tutu Centre, with additional funding through NRF grant 98183. The financial assistance of the NRF through SAEON toward this research is hereby acknowledged. Opinions expressed and conclusions arrived at are those of the authors and are not necessarily to be attributed to the NRF and SAEON. Additional funding from German Federal Ministry for Education and Research (BMBF) framework project SPACES (03G0835A) is also acknowledged. J. V. D acknowledges funding from the Helmholtz Association and the GEOMAR Helmholtz Centre for Ocean Research Kiel (grant IV014/GH018).

References

Arguez, A., Durre, I., Applequist, S., Vose, R. S., Squires, M. F., Yin, X., & Owen, T. W. (2012). NOAA's 1981–2010 U.S. climate normals. *Bulletin of the American Meteorological Society*, *93*(11), 1687–1697. https://doi.org/10.1175/BAMS-D-11-00197.1

Atlas, R., Hoffman, R. N., Ardizzone, J., Leidner, S. M., Jusem, J. C., Smith, D. K., & Gombos, D. (2011). A cross-calibrated, multiplatform ocean surface wind velocity product for meteorological and oceanographic applications. *Bulletin of the American Meteorological Society*, *92*(2), 157–174. https://doi.org/10.1175/2010BAMS2946.1

Barnier, B., Madec, G., Penduff, T., Molines, J. M., Treguier, A. M., Le Sommer, J., & De Cuevas, B. (2006). Impact of partial steps and momentum advection schemes in a global ocean circulation model at eddy-permitting resolution. *Ocean Dynamics*, *56*(5-6), 543–567. https://doi.org/10.1007/s10236-006-0082-1

Beckley, L. E. (1983). Sea-surface temperature variability around Cape Recife, South Africa. *South African Journal of Science*, *79*(December), 436–438.

Blanke, B., Penven, P., Roy, C., Chang, N., & Kokoszka, F. (2009). Ocean variability over the Agulhas Bank and its dynamical connection with the southern Benguela upwelling system. *Journal of Geophysical Research*, *114*, C12028. https://doi.org/10.1029/2009JC005358

Bravo, L., Ramos, M., Astudillo, O., Dewitte, B., & Goubanova, K. (2016). Seasonal variability of the Ekman transport and pumping in the upwelling system off central-northern Chile (∼30°S) based on a high-resolution atmospheric regional model (WRF). *Ocean Science*, *12*, 1049–1065. https://doi.org/10.5194/os-12-1049-2016

Chapman, P., & Largier, J. L. (1989). On the origin of Agulhas Bank bottom water. *South African Journal of Science*, *85*(JANUARY), 515–519.

Chelliah, M., & Ropelewski, C. F. (2000). Reanalyses-based tropospheric temperature estimates: Uncertainties in the context of global climate change detection. *Journal of Climate*, *13*(17), 3187–3205. https://doi.org/10.1175/1520-0442(2000)013<3187:RBTTEU>2.0.CO;2

Chelton, D. B., Deszoeke, R. A., Schlax, M. G., El Naggar, K., & Siwertz, N. (1998). Geographical Variability of the First Baroclinic Rossby Radius of Deformation. *Journal of Physical Oceanography*, *28*(3), 433–460.

Coetzee, J. C., Van Der Lingen, C. D., Hutchings, L., & Fairweather, T. P. (2008). Has the fishery contributed to a major shift in the distribution of South African sardine? *ICES Journal of Marine Science*, *65*(9), 1676–1688. https://doi.org/10.1093/icesjms/fsn184

Conkright, M., Levitus, S., & Boyer, T. P. (1994). NOAA Atlas NESDIS 1. World Ocean Atlas 1994, Volume 1: Nutrients 3 March.

Debreu, L., & Blayo, E. (2008). Two-way embedding algorithms: A review. *Ocean Dynamics*, *58*(5-6), 415–428. https://doi.org/10.1007/s10236-008-0150-9

Dee, D. P., Uppala, S. M., Simmons, A. J., Berrisford, P., Poli, P., Kobayashi, S., & Vitart, F. (2011). The ERA-Interim reanalysis: Configuration and performance of the data assimilation system. *Quarterly Journal of the Royal Meteorological Society*, *137*(656), 553–597. https://doi.org/10.1002/qj.828

Durgadoo, J. V., Loveday, B. R., Reason, C. J. C., Penven, P., & Biastoch, A. (2013). Agulhas leakage predominantly responds to the Southern Hemisphere westerlies. *Journal of Physical Oceanography*, *43*(10), 2113–2131. https://doi.org/10.1175/JPO-D-13-047.1

Goschen, W. S., Schuman, E. H., Bernard, K. S., Bailey, S. E., & Deyzel, S. H. P. (2012). Upwelling and ocean structures off Algoa Bay and the south-east coast of South Africa. *African Journal of Marine Science*, *34*(4), 525–536.

Grémillet, D., Lewis, S., Drapeau, L., Lingen, C. D. V. D., Huggett, J. A., Coetzee, J. C., & Ryan, P. G. (2008). Spatial match-mismatch in the Benguela upwelling zone: Should we expect chlorophyll and sea-surface temperature to predict marine predator distributions? *Journal of Applied Ecology*, *45*, 610–621. https://doi.org/10.1111/j.1365-2664.2007.01447.x

Hill, K. L., Rintoul, S. R., Coleman, R., & Ridgway, K. R. (2008). Wind forced low frequency variability of the East Australia Current. *Geophysical Research Letters*, *35*, L08602. https://doi.org/10.1029/2007GL032912

Hines, K. M., Bromwich, D. H., & Marshall, G. J. (2000). Artificial surface pressure trends in the NCEP-NCAR reanalysis over the southern ocean and Antartica. *Journal of Climate*, *13*(22), 3940–3952. https://doi.org/10.1175/1520-0442(2000)013<3940:ASPTIT>2.0.CO;2

Hutchings, L. (1994). The Aguhas Bank: A synthesis of available information and a brief comparison with other east-coast shelf regions. *South African Journal of Science*, *90*, 179–185.

Hyun, K. H., & He, R. (2010). Coastal upwelling in the South Atlantic Bight: A revisit of the 2003 cold event using long term observations and model hindcast solutions. *Journal of Marine Systems*, *83*(1-2), 1–13. https://doi.org/10.1016/j.jmarsys.2010.05.014

Jackson, J. M., Rainville, L., Roberts, M. J., McQuaid, C. D., & Lutjeharms, J. R. (2012). Mesoscale bio-physical interactions between the Agulhas Current and the Agulhas Bank, South Africa. *Continental Shelf Research*, *49*, 10–24. https://doi.org/10.1016/j.csr.2012.09.005

Kalnay, E., Kanamitsu, M., Kistler, R., Collins, W., Deaven, D., Gandin, L., & Joseph, D. (1996). The NCEP/NCAR 40-year reanalysis project, *77*(3), 437–471. https://doi.org/10.1175/1520-0477(1996)077<0437:TNYRP>2.0.CO;2

Kistler, R., Kalnay, E., Collins, W., Saha, S., White, G., Woollen, J., & Fiorino, M. (2001). The NCEP-NCAR 50-Year Reanalysis: Monthly Means CD-ROM and documentation. *Bulletin of the American Meteorological Society*, *82*, 247–268. https://doi.org/10.1175/1520-0477(2001)082<0247:TNNYRM>2.3.CO;2

Krug, M., Tournadre, J., & Dufois, F. (2014). Interactions between the Agulhas Current and the eastern margin of the Agulhas Bank. *Continental Shelf Research*, *81*, 67–79. https://doi.org/10.1016/j.csr.2014.02.020

Large, W. G., & Yeager, S. G. (2009). The global climatology of an interannually varying air—Sea flux data set. *Climate Dynamics*, *33*(2-3), 341–364. https://doi.org/10.1007/s00382-008-0441-3

Largier, J. L., & Swart, V. P. (1987). East-west variation in thermocline breakdown on the Agulhas Bank. *South African Journal Of Marine Science*, *5*(1), 263–272.

Leber, G. M., Beal, L. M., & Elipot, S. (2016). Wind and current forcing combine to drive strong upwelling in the Agulhas Current. *Journal of Physical Oceanography*, *47*, 123–134. https://doi.org/10.1175/JPO-D-16-0079.1

Lutjeharms, J. (2006). *The Agulhas Current*. Berlin: Springer.

Lutjeharms, J. R. E., Cooper, J., & Roberts, M. (2000). Upwelling at the inshore edge of the Agulhas Current. *Continental Shelf Research*, *20*(7), 737–761. https://doi.org/10.1016/S0278-4343(99)00092-8

Madec, G. (2008). NEMO reference manual, ocean dynamic component: NEMO-OPA. Note du Pôle de modélisation, Institut Pierre Simon Laplace, France.

Malan, N., Backeberg, B., Biastoch, A., Durgadoo, J. V., Samuelsen, A., Reason, C., & Hermes, J. (2018). Agulhas Current Meanders facilitate shelf-slope exchange on the Eastern Agulhas Bank. *Journal of Geophysical Research: Oceans*, *123*, 4762–4778. https://doi.org/10.1029/2017JC013602

Marshall, G. J. (2003). Trends in the Southern Annular Mode from observations and reanalyses. *Journal of Climate*, *16*(24), 4134–4143. https://doi.org/10.1175/1520-0442(2003)016<4134:TITSAM>2.0.CO;2

Morris, T., Hermes, J., Beal, L., Du Plessis, M., Rae, C. D., Gulekana, M., & Ansorge, I. J. (2017). The importance of monitoring the Greater Agulhas Current and its inter-ocean exchanges using large mooring arrays. *South African Journal of Science*, *113*(7-8), 1–7. https://doi.org/10.17159/sajs.2017/20160330

Powell, A. M., & Xu, J. (2011). A new assessment of the mid-1970s abrupt atmospheric temperature change in the NCEP/NCAR reanalysis and associated solar forcing implications. *Theoretical and Applied Climatology*, *104*(3-4), 443–458. https://doi.org/10.1007/s00704-010-0344-1

Raphael, M. N. (2004). A zonal wave 3 index for the Southern Hemisphere. *Geophysical Research Letters*, *31*, L23212. https://doi.org/10.1029/2004GL020365

Reason, C. J. C., & Rouault, M. (2005). Links between the Antarctic Oscillation and winter rainfall over western South Africa. *Geophysical Research Letters*, *32*, L07705. https://doi.org/10.1029/2005GL022419

Reynolds, R. W., Rayner, N. A., Smith, T. M., Stokes, D. C., & Wang, W. (2002). An improved in situ and satellite SST analysis for climate. *Journal of Climate*, *15*(13), 1609–1625. https://doi.org/10.1175/1520-0442(2002)015<1609:AIISAS>2.0.CO;2

Rodionov, S. (2005). A brief overview of the regime shift detection methods. Large-scale disturbances (regime shifts) and recovery in aquatic systems: Challenges for management toward sustainability Table 417–24.

Rouault, M., Penven, P., & Pohl, B. (2009). Warming in the Agulhas Current system since the 1980's. *Geophysical Research Letters*, *36*, L12602. https://doi.org/10.1029/2009GL037987

Rouault, M., Pohl, B., & Penven, P. (2010). Coastal oceanic climate change and variability from 1982 to 2009 around South Africa. *African Journal of Marine Science*, *32*(2), 237–246. https://doi.org/10.2989/1814232X.2010.501563

Roy, C., van der Lingen, C., Coetzee, J., & Lutjeharms, J. (2007). Abrupt environmental shift associated with changes in the distribution of Cape anchovy Engraulis encrasicolus spawners in the southern Benguela. *African Journal of Marine Science*, *29*(3), 309–319. https://doi.org/10.2989/AJMS.2007.29.3.1.331

Schaeffer, A., & Roughan, M. (2017). Subsurface intensification of marine heatwaves off southeastern Australia: The role of stratification and local winds. *Geophysical Research Letters*, *44*, 5025–5033. https://doi.org/10.1002/2017GL073714

Sprintall, J., & Liu, T. W. (2005). Ekman mass and heat transport in the Indonesian Seas. *Oceanography*, *18*(4), 88–97.

Sturaro, G. (2003). A closer look at the climatological discontinuities present in the NCEP/NCAR reanalysis temperature due to the introduction of satellite data. *Climate Dynamics*, *21*, 309–316. https://doi.org/10.1007/s00382-003-0334-4

Swart, V. P., & Largier, J. L. (1987). Thermal structure of Agulhas Bank water. *South African Journal Of Marine Science*, *5*(July 2015), 243–253. https://doi.org/10.2989/025776187784522153

Verheye, H. M., Richardson, A. J., Hutchings, L., Marska, G., & Gianakouras, D. (1998). Long-term trends in the abundance and community structure of coastal zooplankton in the southern Benguela system, 1951–1996. *South African Journal of Marine Science*, *19*(1), 317–332. https://doi.org/10.2989/025776198784126728

Weldon, D., & Reason, C. J. C. (2014). Variability of rainfall characteristics over the South Coast region of South Africa. *Theoretical and Applied Climatology*, *115*(1-2), 177–185. https://doi.org/10.1007/s00704-013-0882-4

Wu, R., & Xie, S. P. (2003). On equatorial Pacific surface wind changes around 1977: NCEP-NCAR reanalysis versus COADS observations. *Journal of Climate*, *16*(1), 167–173. https://doi.org/10.1175/1520-0442(2003)016<0167:OEPSWC>2.0.CO;2